White Rose Research Online

eprints@whiterose.ac.uk
https://eprints.whiterose.ac.uk
Universities of Leeds, Sheffield and York

Deposited via The University of Sheffield.

White Rose Research Online URL for this paper:
https://eprints.whiterose.ac.uk/id/eprint/90249/

Version: Accepted Version

Article:
Chen, Q., Veres, S.M., Wang, Y. et al. (2015) Virtual Spring- Damper Mesh-Based Formation Control for Spacecraft Swarms in Potential Fields. Journal of Guidance, Control, and Dynamics, 38 (3). pp. 539-546. ISSN: 0731-5090

https://doi.org/10.2514/1.G000569

Reuse
Items deposited in White Rose Research Online are protected by copyright, with all rights reserved unless indicated otherwise. They may be downloaded and/or printed for private study, or other acts as permitted by national copyright laws. The publisher or other rights holders may allow further reproduction and re-use of the full text version. This is indicated by the licence information on the White Rose Research Online record for the item.

Takedown
If you consider content in White Rose Research Online to be in breach of UK law, please notify us by emailing eprints@whiterose.ac.uk including the URL of the record and the reason for the withdrawal request.

UNIVERSITY OF LEEDS
University of Sheffield
UNIVERSITY of York

Virtual Spring-Damper Mesh-Based Formation Control for Spacecraft Swarms in Potential Fields

Qifeng Chen[1]
National University of Defense Technology, Changsha, Hunan, 410073, China

Sandor M Veres[2]
University of Sheffield, Sheffield, S13JD, United Kingdom

Yaonan Wang[3]
Hunan University, Changsha, Hunan, 410082, China

and
Yunhe Meng[4]
National University of Defense Technology, Changsha, Hunan, 410073, China

I. Introduction

The goal of formation control is to coordinate a team of agents to maintain a particular geometric pattern or set of relative positions. The behavior of a networked, multi-agent system depends on not only the dynamics of the individual agents but also the interactions between the individual agents [1]. Thus, designing suitable interactions is the main challenge for coordinating multiple agents; local interactions that lead to the required global behaviors are particularly desirable for distributed implementations.

Several distributed formation control architectures have been proposed in the literature. One popular architecture is called leader-following (LF) [2-4]. In the LF architecture, the followers use the leader as their control reference, which provides ease of implementation and analysis. However, the LF architecture has poor disturbance rejection properties because there is no explicit feedback from the followers to the leader [5, 6]. Additionally, the leader is a single point of failure for the entire group [6]. Introducing non-hierarchical connections and feedbacks to the control interaction architecture is expected to result in a better performance and to distribute the control effort more evenly among the agents [7]. The cyclic architecture [4, 7] provides feedbacks, but the connecting topologies and the formation shapes that can be realized are rather restricted. Fax and Murray [5] considered a broad range of interconnection possibilities for vehicle with linear dynamics and proved a Nyquist criterion to determine the effect of the communication topology on the formation's stability. The passivity-based approach [8] exploits the fact that the closed-loop system inherits the passivity properties of its components when the information flow is bidirectional.

[1] Associate Professor, College of Aerospace Science and Engineering; cqf_nudt@yahoo.com.
[2] Professor, Department of Automatic Control and Systems Engineering.
[3] Professor, College of Electrical and Information Engineering.
[4] Associate Professor, College of Aerospace Science and Engineering.

Thus the stability of coordinated control of multiple agents is achieved through passivity. The behavioral approach [4] combines the outputs of multiple controllers designed for achieving different behaviors. This approach is flexible in formation control design but is difficult to analyze mathematically [9]. In the virtual structure approach [4, 9], the desired formation is considered a virtual rigid body, and the agents track the trajectories generated by the motion of the rigid body. In the consensus-based approach [10], consensus protocols are designed to reach agreement on the value of the formation variables.

For most of the distributed formation control methods presented in the literature, a basic assumption is that every agent knows its own position or velocity. However, for spacecraft formation missions, accurate absolute position measurements are often not available, whereas relative measurements can reach much higher accuracy; besides the absolute positions of spacecraft are usually not subject to as stringent constraints as the relative positions are. Thus, it is reasonable to control relative motion using only relative measurements [11]. In addition, spacecraft dynamics within the gravitational field has not been considered for these distributed control methods.

This paper derives a distributed control method based on a virtual spring-damper mesh (VSDM) for the formation control of spacecraft swarms in a gravitational potential field. This method requires no information about the absolute positions or velocities of spacecraft. Bidirectional local interaction, which provides intrinsic feedback, is used, and general connected topologies are assumed. Collision avoidance and topology switching are integrated, and the convergence of the closed-loop system is assured. Approximate expressions that predict the steady-state performance of relative position errors and control accelerations are also derived by linearization and using algebraic graph representations. The VSDM method proposed in this paper is different from the virtual spring mesh algorithm explored for the deployment of mobile sensors in Ref. [12]. One spring and one damper are combined as a connection unit for relative motion control in this study, whereas in Ref. [12], virtual dampers are separately used to decrease the absolute velocity of each agent to a stationary state.

This paper is organized as follows. In Sec. II, a graphic description for the relative motion in a formation is briefly introduced. In Sec. III, the VSDM control law is presented, and the convergence and steady-state performance for VSDM-based spacecraft formation control are analyzed. In Sec. IV, collision avoidance is integrated with VSDM-based formation control. In Sec. V, the switching of the connecting topology in the VSDM-based formation control is investigated. In Sec. VI, the effectiveness of the proposed method is demonstrated via numerical simulations. Finally, in Sec. VII some concluding remarks are provided.

II. Graphic Description for the Relative Motion in a Formation

The relative states between the agents in a formation can be associated with the incidence matrix of a directed graph (or digraph) $G=(V,E)$, where $V=\{v_1,v_2,\cdots,v_n\}$ is the vertex set corresponding to the n agents and $E=\{(v_i,v_j)\,|\,v_i,v_j\in V;i\neq j\}$ is the edge set (all graphs have n vertices in this paper). If $(v_i,v_j)\in E$, then v_i and v_j are adjacent; i.e., they are neighbors to each other. Any edge $e_k=(v_i,v_j)\in E$ of the digraph is an ordered pair. The starting vertex v_i is defined to be the tail of the edge, and the ending vertex v_j is the head. The incidence matrix of the digraph G is defined as follows [1]:

$$\boldsymbol{D}(G)=[d_{ik}],\quad \text{where } d_{ik}=\begin{cases}-1 & \text{if } v_i \text{ is the tail of } e_k\\ 1 & \text{if } v_i \text{ is the head of } e_k\\ 0 & \text{otherwise}\end{cases} \tag{1}$$

The columns of the incidence matrix represent the edges of the digraph. Note that $\boldsymbol{D}(G)^T\boldsymbol{1}_n=\boldsymbol{0}$, where $\boldsymbol{1}_n$ is the $n\times 1$ column vector with a value of 1 for every entry. The relative position vector corresponding to the k-th directed edge $e_k=(v_i,v_j)$ of the digraph G can be defined as

$$\boldsymbol{p}_k=\boldsymbol{r}_{ji}=\boldsymbol{r}_j-\boldsymbol{r}_i=\left(\boldsymbol{D}(e_k)^T\otimes\boldsymbol{I}_3\right)R \tag{2}$$

where $\boldsymbol{r}_i=[x_i,y_i,z_i]^T$ is the position vector of the i-th agent, $R=[\boldsymbol{r}_1^T,\boldsymbol{r}_2^T,\cdots,\boldsymbol{r}_n^T]^T$, $\otimes$ denotes the Kronecker product, and $\boldsymbol{D}(e_k)$ denotes the k-th column of $\boldsymbol{D}(G)$, where a slight abuse of notation is used. Therefore, the relative positions corresponding to the edges of the digraph G can be represented in vector form as

$$P_G=\left(\boldsymbol{D}(G)^T\otimes\boldsymbol{I}_3\right)R \tag{3}$$

where $P_G=[\boldsymbol{p}_1^T,\boldsymbol{p}_2^T,\cdots,\boldsymbol{p}_m^T]^T$ and m is the number of edges in G. The minimum and complete set of independent relative positions of an n-agent system can be specified by a directed spanning tree G_T as

$$P=\left(\boldsymbol{D}(G_T)^T\otimes\boldsymbol{I}_3\right)R \tag{4}$$

where $P=\left[\boldsymbol{p}_1^T,\boldsymbol{p}_2^T,\cdots,\boldsymbol{p}_{n-1}^T\right]^T$. The notations of the graph Laplacian, $\boldsymbol{L}(G)=\boldsymbol{D}(G)\boldsymbol{D}(G)^T$, and the edge Laplacian [1], $\boldsymbol{L}_e(G)=\boldsymbol{D}(G)^T\boldsymbol{D}(G)$ are used in this paper. The edge Laplacian of a spanning tree is an invertible matrix.

There exists a linear transformation from any directed spanning tree G_T to any digraph G, such that [1]

$$\boldsymbol{D}(G)^T=\boldsymbol{T}\boldsymbol{D}(G_T)^T,\quad \boldsymbol{T}=\boldsymbol{D}(G)^T\boldsymbol{D}(G_T)\boldsymbol{L}_e(G_T)^{-1} \tag{5}$$

Thus, the relation between P_G and P can be obtained as

$$P_G=(\boldsymbol{T}\otimes\boldsymbol{I}_3)P \tag{6}$$

For a weakly connected digraph G and its spanning tree subgraph G_T', there exists an $(n-1)\times q$ matrix $\boldsymbol{\psi}$ such that [1]

$$\boldsymbol{D}(G)=\boldsymbol{D}(G_T')\left[\boldsymbol{I}_{n-1}\quad\boldsymbol{\psi}\right] \tag{7}$$

where q is the number of edges that are in G but not in G_T'. If the complete graph κ_n is considered in the transformation of Eq. (5), by noting that $\boldsymbol{L}(\kappa_n)=n\boldsymbol{I}_n-\boldsymbol{1}_n\boldsymbol{1}_n^T$, a relation can be derived as

$$\boldsymbol{D}(G_T)\boldsymbol{L}_e^{-1}(G_T)\boldsymbol{D}(G_T)^T=\frac{1}{n}\boldsymbol{L}(\kappa_n)=\boldsymbol{I}_n-\frac{1}{n}\boldsymbol{1}_n\boldsymbol{1}_n^T \tag{8}$$

The transformations between G_T and G_T' can be defined from Eq. (5) as

$$\begin{aligned}\boldsymbol{D}(G_T')^T&=\boldsymbol{T}_t\boldsymbol{D}(G_T)^T,\quad \boldsymbol{T}_t=\boldsymbol{D}(G_T')^T\boldsymbol{D}(G_T)\boldsymbol{L}_e(G_T)^{-1}\\ \boldsymbol{D}(G_T)^T&=\boldsymbol{T}_t'\boldsymbol{D}(G_T')^T,\quad \boldsymbol{T}_t'=\boldsymbol{D}(G_T)^T\boldsymbol{D}(G_T')\boldsymbol{L}_e(G_T')^{-1}\end{aligned} \tag{9}$$

It can be verified that $\boldsymbol{T}_t\boldsymbol{T}_t'=\boldsymbol{T}_t'\boldsymbol{T}_t=\boldsymbol{I}_{n-1}$ using Eq. (9) and (8).

III. Virtual Spring-Damper Mesh-Based Spacecraft Formation Control

A. Model Setup

Consider a swarm of spacecraft in a gravitational field. Each spacecraft is considered a point with unit mass. The translational motion of the i-th spacecraft is described as

$$\ddot{\boldsymbol{r}}_i=-\nabla Q(\boldsymbol{r}_i)+\boldsymbol{a}_i\qquad(i=1,2,\cdots,n) \tag{10}$$

where Q is the potential function of the gravitational field and $\boldsymbol{a}_i$ is the control acceleration. For the spacecraft formation application in low Earth orbit, this model can account for the zonal gravitational harmonics of the

perturbing potential of the oblateness of the Earth. For example, when the main perturbation, the J_2 term from the oblateness of the Earth, is included, the gravitational potential function is as follows [14]:

$$Q(\boldsymbol{r}) = -\frac{\mu}{\sqrt{x^2+y^2+z^2}}\left[1-\frac{R_e^2}{2\left(x^2+y^2+z^2\right)}\left(3\frac{z^2}{x^2+y^2+z^2}-1\right)J_2\right] \tag{11}$$

where $\boldsymbol{r} = \left[x, y, z\right]^T$ is the position vector in the Earth-centered inertial (ECI) reference frame, R_e is the mean equatorial radius of the Earth, μ is the gravitational constant of the Earth, and

$$\mu = 3.986004405\times10^{14}\,\mathrm{m^3 s^{-2}},\quad R_e = 6378137\,\mathrm{m},\quad J_2 = 1.082626675\times10^{-3}.$$

B. The VSDM Control Law

Consider a system of point masses connected by a spring-damper mesh as shown in Fig. 1. All of the springs and dampers have zero mass. The natural lengths of the springs are set to be the desired distances between the point masses. Because of the elastic and damping forces, the system will eventually reach an equilibrium, i.e., the desired configuration of the relative motions of these point masses. It is reasonable to expect that the spring-damper mesh works for a system of agents in a general dynamical environment. The VSDM method is an analog to the spring-damper mesh system. No actual springs or dampers are used, but the control forces that drive the agents are generated based on virtual spring-damper pairs "connected" to the agents.

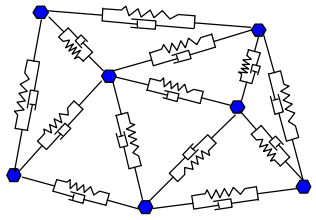

Fig. 1 Point masses connected by a spring-damper mesh.

This paper considers a linear, relative-state-based VSDM control law. The spring-damper mesh in 3-D space is "projected" onto the three axes of a shared coordinate frame. For each adjacent agent pair in the connecting topology, three independent connections are assumed, each parallel to one of the coordinate axes. In this way, the control inputs are proportional to the relative states between the agents:

$$\boldsymbol{u}_i = -k_s\sum_{j\in N_i}\left(\boldsymbol{r}_i-\boldsymbol{r}_j-\boldsymbol{r}_{ij}^d\right)-k_d\sum_{j\in N_i}\left(\dot{\boldsymbol{r}}_i-\dot{\boldsymbol{r}}_j\right)\qquad \left(i=1,2,\cdots,n\right) \tag{12}$$

where N_i is the index set of those agents adjacent to the *i*-th agent, $\boldsymbol{r}_{ij}^d$ is the desired relative position between agent *i* and agent *j*, $\dot{\boldsymbol{r}}_i = \left[\dot{x}_i, \dot{y}_i, \dot{z}_i\right]^T$ is the velocity of agent *i*, $k_s > 0$ is the elastic coefficient of the springs, and $k_d > 0$ is the damping coefficient. The superscript "*d*" means "desired value" throughout the remainder of this paper.

The control input for agent *i* in (12) can be reformulated using the edges in the connecting graph *G* as

$$\boldsymbol{u}_i = -\sum_{e_k \in E} k_s d_{ik} \left(\boldsymbol{p}_k - \boldsymbol{p}_k^d\right) - \sum_{e_k \in E} k_d d_{ik} \dot{\boldsymbol{p}}_k \qquad \left(i = 1,2,\cdots,n\right) \tag{13}$$

Rewriting Eq. (13) in matrix form and using the definition of the incidence matrix, the VSDM control law becomes

$$U = -k_s \left(\boldsymbol{D}\left(G\right) \otimes \boldsymbol{I}_3\right)\left(P_G - P_G^d\right) - k_d \left(\boldsymbol{D}\left(G\right) \otimes \boldsymbol{I}_3\right)\dot{P}_G \tag{14}$$

where $U = \left[\boldsymbol{u}_1^T, \boldsymbol{u}_2^T, \cdots, \boldsymbol{u}_n^T\right]^T$.

In the VSDM method, each connection is double-sided. Thus, the connecting topologies are undirected. In Eq. (14) and throughout this paper, the definition of the incidence matrix is slightly modified to fit the case of undirected graphs. For an undirected graph *G*, its incidence matrix $\boldsymbol{D}\left(G\right)$ represents the incidence matrix of a derived digraph by endowing every edge of *G* with an arbitrary orientation. However, the same digraph derived from *G* must be used in specifying P_G, P_G^d, and $\boldsymbol{D}\left(G\right)$.

To implement the VSDM-based distributed control law, a common inertial coordinate frame must be used by each agent. Because the VSDM control law utilizes only the relative states between agents, the location of the origin of the coordinate frame does not matter, and local frames can be used. However, each agent must be able to determine its attitude with respect to the common coordinate frame. Each agent must obtain the relative positions and the relative velocities of adjacent agents either by using the measurements from itself or by using the communication of measurements from adjacent agents. Spacecrafts are required to exert continuously variable control accelerations, which may cause difficulties for implementation using conventional thrusters, although recent generations of ion thruster [15] and variable specific impulse plasma thrusters [16] hold great promise to fulfill this role.

C. Convergence of the Closed-loop System

Theorem III.1 For a spacecraft swarm with the dynamics of Eq. (10) under the VSDM-based formation control of Eq. (12), if the connecting topology G is connected, then the velocities of the spacecraft in the swarm become equal as $t \to \infty$.

Proof: Consider the energy function

$$\bar{V} = \frac{1}{2}\sum_{i=1}^{n} \dot{\boldsymbol{r}}_i \cdot \dot{\boldsymbol{r}}_i + \sum_{i=1}^{n}\left(Q\left(\boldsymbol{r}_i\right) - Q_0\right) + \frac{1}{2}\sum_{k=1}^{m} k_s \left(\boldsymbol{p}_k - \boldsymbol{p}_k^d\right)\cdot\left(\boldsymbol{p}_k - \boldsymbol{p}_k^d\right) > 0 \tag{15}$$

where Q_0 is a negative constant satisfying $Q\left(\boldsymbol{r}_i\right) - Q_0 > 0$ for the trajectories of $\boldsymbol{r}_i\left(t\right)$ $\left(i = 1,2,\mathrm{L}\ ,n\right)$. For the spacecraft formation flying problems considered in this paper, all of the spacecraft are very close to a natural reference orbit. The gravity potential $Q\left(\boldsymbol{r}_i\right)$s are bounded during the spacecraft motion. Thus, it is always possible to find such a Q_0. Then,

$$\begin{aligned}
\dot{\bar{V}} &= \sum_{i=1}^{n} \dot{\boldsymbol{r}}_i \cdot \ddot{\boldsymbol{r}}_i + \sum_{i=1}^{n} \nabla Q\left(\boldsymbol{r}_i\right)\cdot \dot{\boldsymbol{r}}_i + \sum_{k=1}^{m} k_s \left(\boldsymbol{p}_k - \boldsymbol{p}_k^d\right)\cdot \dot{\boldsymbol{p}}_k \\
&= \sum_{i=1}^{n} \dot{\boldsymbol{r}}_i \cdot \left[\ddot{\boldsymbol{r}}_i + \nabla Q\left(\boldsymbol{r}_i\right) + k_s \sum_{j\in N_i}\left(\boldsymbol{r}_i - \boldsymbol{r}_j - \boldsymbol{r}_{ij}^d\right)\right] \\
&= -k_d \sum_{i=1}^{n} \dot{\boldsymbol{r}}_i \cdot \sum_{j\in N_i}\left(\dot{\boldsymbol{r}}_i - \dot{\boldsymbol{r}}_j\right)
\end{aligned}$$

which yields

$$\dot{\bar{V}} = -k_d \sum_{k=1}^{m} \dot{\boldsymbol{p}}_k \cdot \dot{\boldsymbol{p}}_k \le 0 \tag{16}$$

Therefore, according to LaSalle's invariance principle [17], each $\dot{\boldsymbol{p}}_k$, which is the relative velocity between the two vertices of edge $e_k \in E$, approaches zero as $t \to \infty$. Considering that the connecting topology G is connected, Theorem III.1 is thus proven. □

D. Analysis of Steady-State Performance

In this subsection, the analytical results for the steady-state errors and control accelerations are presented. According to Theorem III.1, for $\forall i, j$, $\dot{\boldsymbol{r}}_i = \dot{\boldsymbol{r}}_j$, $\boldsymbol{r}_i - \boldsymbol{r}_j = const$, and $\ddot{\boldsymbol{r}}_i - \ddot{\boldsymbol{r}}_j = 0$ when $t \to \infty$. Therefore, the equilibrium for the relative motion of the swarm can be obtained by solving the nonlinear equation $\ddot{P} = 0$. Note that

for spacecraft formation flying problems, $\boldsymbol{r}_i - \boldsymbol{r}_j$ and $\boldsymbol{r}_{ij}^d$ are very small relative to $\boldsymbol{r}_i$ and $\boldsymbol{r}_j$ $\left(i, j = 1,2,\cdots,n; i \neq j\right)$; therefore, the linearization of the dynamics is used to facilitate the analysis.

Suppose $\boldsymbol{r}_0$ stands for the motion of the reference point, where the motions of the spacecraft in the swarm are all very close to the reference point. By linearizing the dynamics and noting that $\dot{\boldsymbol{r}}_i = \dot{\boldsymbol{r}}_j$ at steady state ($t \to \infty$), the swarm motion of Eq. (10) under the VSDM control of Eq. (12) at steady state are obtained in vector form as

$$\ddot{R} = \boldsymbol{1}_n \otimes \left[\nabla^2 Q\left(\boldsymbol{r}_0\right)\boldsymbol{r}_0 - \nabla Q\left(\boldsymbol{r}_0\right)\right] - \left[\boldsymbol{I}_n \otimes \nabla^2 Q\left(\boldsymbol{r}_0\right)\right]R - k_s\left[\boldsymbol{D}\left(G\right) \otimes \boldsymbol{I}_3\right]\left(P_G - P_G^d\right) \tag{17}$$

Substituting Eq. (17) into the twice differentiated Eq. (4) with respect to time, one obtains

$$\ddot{P} = -\left[\boldsymbol{D}\left(G_T\right)^T \otimes \nabla^2 Q\left(\boldsymbol{r}_0\right)\right]R - k_s\left[\boldsymbol{D}\left(G_T\right)^T \boldsymbol{D}\left(G\right) \otimes \boldsymbol{I}_3\right]\left(P_G - P_G^d\right)$$

Substituting Eqs. (4), (5), and (6) and solving the equation $\ddot{P} = 0$ yields

$$P - P^d = -\frac{1}{k_s}\left\{\boldsymbol{L}_e\left(G_T\right)\left[\boldsymbol{D}\left(G_T\right)^T \boldsymbol{D}\left(G\right)\boldsymbol{D}\left(G\right)^T \boldsymbol{D}\left(G_T\right)\right]^{-1} \otimes \nabla^2 Q\left(\boldsymbol{r}_0\right)\right\}P \tag{18}$$

From Eqs. (7) and (9) it can be obtained that

$$\boldsymbol{D}\left(G_T\right)^T \boldsymbol{D}\left(G\right)\boldsymbol{D}\left(G\right)^T \boldsymbol{D}\left(G_T\right) = \boldsymbol{T}_t'\boldsymbol{L}_e\left(G_T'\right)\left(\boldsymbol{I}_{n-1} + \boldsymbol{\psi}\boldsymbol{\psi}^T\right)\boldsymbol{T}_t\boldsymbol{L}_e\left(G_T\right) \tag{19}$$

Eq. (19) verifies the invertibility of the matrix $\boldsymbol{D}\left(G_T\right)^T \boldsymbol{D}\left(G\right)\boldsymbol{D}\left(G\right)^T \boldsymbol{D}\left(G_T\right)$ in Eq. (18). Eq. (18) shows that the steady-state error between the relative position vector of the swarm P and the desired relative position vector P^d can be sufficiently small, if the elastic coefficient k_s is sufficiently large. Thus, if a sufficiently large k_s is used, a good approximation of the relative position errors of the steady-state motion can be

$$P - P^d = -\frac{1}{k_s}\left\{\boldsymbol{L}_e\left(G_T\right)\left[\boldsymbol{D}\left(G_T\right)^T \boldsymbol{D}\left(G\right)\boldsymbol{D}\left(G\right)^T \boldsymbol{D}\left(G_T\right)\right]^{-1} \otimes \nabla^2 Q\left(\boldsymbol{r}_0\right)\right\}P^d \tag{20}$$

Next, the steady-state control acceleration is investigated. At steady state, it holds that $\dot{P}_G = 0$. Substituting Eqs. (6) and (20) into Eq. (14) yields the steady-state control acceleration of the swarm:

$$U = \left\{\boldsymbol{D}\left(G\right)\boldsymbol{T}\boldsymbol{L}_e\left(G_T\right)\left[\boldsymbol{D}\left(G_T\right)^T \boldsymbol{D}\left(G\right)\boldsymbol{D}\left(G\right)^T \boldsymbol{D}\left(G_T\right)\right]^{-1} \otimes \nabla^2 Q\left(\boldsymbol{r}_0\right)\right\}P^d$$

Substituting Eqs. (5), (7), (8), (9), and (19) yields

$$U = \left[\boldsymbol{D}\left(G_T\right)\boldsymbol{L}_e^{-1}\left(G_T\right) \otimes \nabla^2 Q\left(\boldsymbol{r}_0\right)\right]P^d \tag{21}$$

Substituting $P^d = \left(\boldsymbol{D}\left(G_T\right)^T \otimes \boldsymbol{I}_3\right)R^d$, where R^d represents the absolute motion of the swarm that maintains the relative states P^d between spacecraft, and Eq. (8) into Eq. (21) yields

$$\boldsymbol{u}_i = \nabla^2 Q\left(\boldsymbol{r}_0\right)\left(\boldsymbol{r}_i^d - \boldsymbol{r}_c^d\right) \quad \left(i = 1,2,\mathrm{L}\ ,n\right) \tag{22}$$

where $\boldsymbol{r}_c^d = \frac{1}{n}\sum_{j=1}^{n}\boldsymbol{r}_j^d$ is the position of the geometric center of the desired configuration. Eq. (22) shows that the approximate steady-state control accelerations depend only on the desired relative configuration and the gravitational potential function of the reference orbit and that they can thus be predicted before implementation. The elastic coefficient k_s, which is inversely proportional to the control accuracy, does not affect the steady-state control acceleration. This finding means that it is possible to achieve a higher level of accuracy in maintaining a formation without increasing fuel consumption.

IV. Integrating Collision Avoidance

In this section, the integration of an artificial potential function method with the VSDM-based formation control to avoid collisions is investigated. It is assumed that two spacecraft will collide if their distances are smaller than a certain value l_0. The artificial potential function $\varphi(l)$ depends on the distance l between agents. It is a smooth, nonnegative function in $\left(l_0,+\infty\right)$, $\varphi(l) \equiv 0$ when $l \in \left[d,+\infty\right)$, $\varphi(l)$ is monotonically decreasing in $\left(l_0,d\right)$, and $\varphi(l) \to +\infty$ as $l \to l_0^+$, where d ($d > l_0$) is the maximum influence distance of the artificial potential function. The artificial potential function is used as a signal to generate rapidly increasing repulsive forces as the distance decreases. Let $\varphi_{ij} \triangleq \varphi(l_{ij})$ denote the artificial potential function introduced between agent i and agent j, where $i, j = 1,2,\mathrm{L}\ ,n$ and $i \neq j$. The collision avoidance acceleration of agent i is

$$\boldsymbol{u}_i^{ca} = -\sum_{j \neq i}\nabla_{\boldsymbol{r}_i}\varphi_{ij} = -\sum_{j \neq i}\varphi'\left(l_{ij}\right)\frac{1}{l_{ij}}\left(\boldsymbol{r}_i - \boldsymbol{r}_j\right) \tag{23}$$

where $\varphi'\left(l\right) = d\varphi/dl$.

The collision avoidance accelerations that are introduced do not affect the closed-loop convergence for the VSDM-based formation control. Adding the nonnegative artificial potential term $\Phi\left(\boldsymbol{r}_1,\boldsymbol{r}_2,\cdots,\boldsymbol{r}_n\right) = \sum_{i=1}^{n-1}\sum_{j=i+1}^{n}\varphi_{ij}$ to the previously defined energy function in Eq. (15) yields

$$\bar{V} = \frac{1}{2}\sum_{i=1}^{n} \dot{\boldsymbol{r}}_i \cdot \dot{\boldsymbol{r}}_i + \sum_{i=1}^{n} \left(Q\left(\boldsymbol{r}_i\right) - Q_0 \right) + \frac{1}{2}\sum_{k=1}^{m} k_s \left(\boldsymbol{p}_k - \boldsymbol{p}_k^d \right) \cdot \left(\boldsymbol{p}_k - \boldsymbol{p}_k^d \right) + \Phi\left(\boldsymbol{r}_1, \boldsymbol{r}_2, \cdots, \boldsymbol{r}_n\right) > 0 \tag{24}$$

Then, noting that

$$\dot{\Phi}\left(\boldsymbol{r}_1, \boldsymbol{r}_2, \cdots, \boldsymbol{r}_n\right) = \sum_{i=1}^{n-1} \sum_{j=i+1}^{n} \left(\dot{\boldsymbol{r}}_i \cdot \nabla_{\boldsymbol{r}_i} \varphi_{ij} + \dot{\boldsymbol{r}}_j \cdot \nabla_{\boldsymbol{r}_j} \varphi_{ij} \right) = \sum_{i=1}^{n} \dot{\boldsymbol{r}}_i \cdot \sum_{j \neq i} \nabla_{\boldsymbol{r}_i} \varphi_{ij}$$

and $\boldsymbol{a}_i$ in Eq. (10) is the sum of $\boldsymbol{u}_i$ in Eq. (12) and $\boldsymbol{u}_i^{ca}$ in Eq. (23), one obtains

$$\begin{aligned} \dot{\bar{V}} &= \sum_{i=1}^{n} \dot{\boldsymbol{r}}_i \cdot \left[\ddot{\boldsymbol{r}}_i + \nabla Q\left(\boldsymbol{r}_i\right) + k_s \sum_{j \in N_i} \left(\boldsymbol{r}_i - \boldsymbol{r}_j - \boldsymbol{r}_{ij}^d \right) + \sum_{j \neq i} \nabla_{\boldsymbol{r}_i} \varphi_{ij} \right] \\ &= -k_d \sum_{i=1}^{n} \dot{\boldsymbol{r}}_i \cdot \sum_{j \in N_i} \left(\dot{\boldsymbol{r}}_i - \dot{\boldsymbol{r}}_j \right) \end{aligned}$$

which yields Eq. (16). Thus, the same conclusion as Theorem III.1 can be drawn.

Because agents will surely not collide in the desired configuration, the artificial potentials must be designed to generate zero acceleration when the motion of the agents approaches the desired configuration. Thus, the artificial potentials have no effect on the steady-state motion and do not affect the steady-state performance of the VSDM-based formation control.

V. Switching of the Connecting Topology

For formation initialization or reconfiguration missions, the relative positions between agents vary greatly. Improper physical geometry of the connecting topology may occur, which can cause difficulties in implementation, such as blocking of the lines of sight, interference of the transmission signals, or becoming out of sensing and communication range. Therefore, switching to a new connecting topology with a better physical geometry is desirable. The new connecting topology should also be connected. However, switching topologies induces abrupt changes in the elastic energy. This may cause instability in the system. This section develops a criterion that can be verified in a distributed manner for topology switching in the VSDM formation control to ensure convergence. Gabriel graphs are used as a simple way to maintain the connectivity and a favorable physical geometry of the topology.

A. Switching Criteria to Ensure Stability

Let $\sigma(\tau):[0,\infty)\to S$ denote the switching signal, where S is the set of topology indices. τ_k are the switching times at which $\sigma(\tau)$ is discontinuous, where $k=0,1,2,\mathrm{L}$ and $\tau_{k+1}>\tau_k>0$. $G_{\sigma(\tau)}$ is the connecting topology at time τ. To simplify our notation, $G_k=(V,E_k)$ is used to denote the topology in $[\tau_k,\tau_{k+1})$. It is assumed that G_k is connected for all $k=0,1,2,\mathrm{L}$. An energy function of the system under topology switching can be defined as

$$\bar{V}_{\sigma(\tau)}=\frac{1}{2}\sum_{i=1}^{n}\dot{\boldsymbol{r}}_i\cdot\dot{\boldsymbol{r}}_i+\sum_{i=1}^{n}\left(Q(\boldsymbol{r}_i)-Q_0\right)+\frac{1}{2}k_s\sum_{(i,j)\in E_{\sigma(\tau)}}\left(\boldsymbol{r}_i-\boldsymbol{r}_j-\boldsymbol{r}_{ij}^d\right)\cdot\left(\boldsymbol{r}_i-\boldsymbol{r}_j-\boldsymbol{r}_{ij}^d\right)+\Phi(\boldsymbol{r}_1,\boldsymbol{r}_2,\cdots,\boldsymbol{r}_n)\quad(25)$$
$$>0$$

During the time intervals between switching, the energy function continues to smoothly decrease, as shown in Sec. IV:

$$\dot{\bar{V}}_k=-k_d\sum_{(i,j)\in E_k}\left(\dot{\boldsymbol{r}}_i-\dot{\boldsymbol{r}}_j\right)\cdot\left(\dot{\boldsymbol{r}}_i-\dot{\boldsymbol{r}}_j\right)\le 0\quad(26)$$

where $\bar{V}_k$ is the energy function defined in Eq. (24) when the connecting graph is G_k. At the switching times, however, the energy function of the system is discrete and not differentiable. According to the theory of switched systems [18], as long as the value of the energy function at the switching times, i.e., $\bar{V}_{\sigma(\tau_k)}$, continues to decrease, the closed-loop system of the VSDM-based formation control with topology switching is convergent such that the velocities of the spacecraft approach equality. The convergence condition can also be described as a case in which the decrease of the energy function in the time interval (τ_k,τ_{k+1}) is larger than the increase of the elastic energy caused by topology switching at time τ_{k+1}, i.e.,

$$\begin{aligned}\Delta\bar{V}_{k+1}=&\frac{1}{2}k_s\sum_{(i,j)\in E_{k+1}}\left(\boldsymbol{r}_i-\boldsymbol{r}_j-\boldsymbol{r}_{ij}^d\right)\cdot\left(\boldsymbol{r}_i-\boldsymbol{r}_j-\boldsymbol{r}_{ij}^d\right)-\frac{1}{2}k_s\sum_{(i,j)\in E_k}\left(\boldsymbol{r}_i-\boldsymbol{r}_j-\boldsymbol{r}_{ij}^d\right)\cdot\left(\boldsymbol{r}_i-\boldsymbol{r}_j-\boldsymbol{r}_{ij}^d\right)\\&-k_d\int_{\tau_k}^{\tau_{k+1}}\sum_{(i,j)\in E_k}\left(\dot{\boldsymbol{r}}_i-\dot{\boldsymbol{r}}_j\right)\cdot\left(\dot{\boldsymbol{r}}_i-\dot{\boldsymbol{r}}_j\right)dt\le 0\end{aligned}\quad(27)$$

for all $k=0,1,2,\mathrm{L}$. Eq. (27) can be used as an additional condition for implementing topology switching for VSDM-based formation control. The integration in Eq. (27) can be calculated numerically.

The calculation of $\Delta\bar{V}_{k+1}$ can be distributed to each agent as

$$\Delta \bar{V}_{k+1} = \sum_{i=1}^{n} \Delta \bar{V}_{k+1}^{i}$$

$$\Delta \bar{V}_{k+1}^{i} = \frac{1}{4} k_s \left[\sum_{j \in N_i^{k+1}} \left(\boldsymbol{r}_i - \boldsymbol{r}_j - \boldsymbol{r}_{ij}^{d} \right) \cdot \left(\boldsymbol{r}_i - \boldsymbol{r}_j - \boldsymbol{r}_{ij}^{d} \right) - \sum_{j \in N_i^{k}} \left(\boldsymbol{r}_i - \boldsymbol{r}_j - \boldsymbol{r}_{ij}^{d} \right) \cdot \left(\boldsymbol{r}_i - \boldsymbol{r}_j - \boldsymbol{r}_{ij}^{d} \right) \right] \tag{28}$$

$$- \frac{1}{2} k_d \int_{\tau_k}^{\tau_{k+1}} \sum_{j \in N_i^{k}} \left(\dot{\boldsymbol{r}}_i - \dot{\boldsymbol{r}}_j \right) \cdot \left(\dot{\boldsymbol{r}}_i - \dot{\boldsymbol{r}}_j \right) dt$$

where N_i^k is the set of vertices in G_k that are neighbors to v_i. It is obvious that $\Delta \bar{V}_{k+1}^{i}$ can be calculated by agent *i* using only local information. If the connecting topologies are connected and the communication is fast enough, then each agent is able to obtain the $\Delta \bar{V}_{k+1}^{i}$ values calculated by all of the other agents. Thus, the topology switching criteria of Eq. (27) can be verified in a distributed manner.

B. Topology Switching Using Gabriel Graph

A graph is a Gabriel graph [19] if and only if for any of its edges $\left(v_i, v_j \right) \in E$ and $\forall v_k \in V \setminus \left\{ v_i, v_j \right\}$, $d_{ij}^2 < d_{ik}^2 + d_{jk}^2$ is satisfied, where d_{ij} represents the Euclidean distance between v_i and v_j. There are favorable characteristics for the Gabriel graph to be used in topology switching. First, Gabriel graphs are connected. Second, Gabriel graph can be uniquely determined if the relative positions of vertices are given. This ensures consistency in the topology that is determined by each agent, provided that each agent knows the whole relative position information of the swarm. Third, Gabriel graphs have favorable geometric properties. Edges that are nearly parallel on the same vertex are rare, and the chances of interference and block-out are thus also rare.

In the Gabriel graph-based topology switching method, each connecting topology G_k for $k = 0,1,2,\mathrm{L}$ is a Gabriel graph determined by the relative position information of the swarm at the time instant when the connecting topology switches to G_k. At each time instant, the spacecraft check the switching criterion of Eq. (27) through distributed computing and communicating of $\Delta \bar{V}_{k+1}^{i}$s in Eq. (28). If Eq. (27) is satisfied, then the agents consistently switch the topology to the new Gabriel graph determined by the current relative positions of the swarm. Otherwise, the previous connecting topology is maintained. Details about Gabriel graphs and Gabriel graph-based switching can be observed in Refs. [19] and [12], respectively.

VI. Numerical Simulations

A sparse aperture application in low Earth orbit was simulated to assess the performance of the VSDM method. Thirty spacecraft were required to form a sparse aperture on a three-dimensional parabolic surface. The planar layout of the spacecraft on the axial projection of the parabolic surface followed the Golomb pattern [20]. The two most distant spacecraft (longest baseline) were 1000 meters apart. The distance from the vertex to the focus of the parabola was 300 meters. The spacecraft were near a circular reference orbit at an altitude of 500 km. At the initial time, the inclination of the reference orbit was 30°, the right ascension of the ascending node was 60°, and the argument of the perigee and the mean anomaly were both 0°. The initial states of the spacecraft were randomly generated with the relative position to the reference point uniformly distributed in [-500, 500] m along the three coordinate axes in the ECI reference frame. The simulations were carried out by numerical integration. Orbital dynamics with a J_2 perturbing potential of Eq. (11) were used. The MATLAB built-in function ode45 was used for the numerical integrations. The relative tolerance and the absolute tolerance were both set to 10^{-10}.

A simple, segmented linear tuning policy of the elastic and the damping coefficients is used. When the configuration error is large at the beginning of the simulation, small coefficients are used to avoid high control thrust levels. As the simulation continues, the error becomes smaller, and larger coefficients are used to reduce the errors. The tuning of the coefficients with respect to time is shown in Fig. 2.

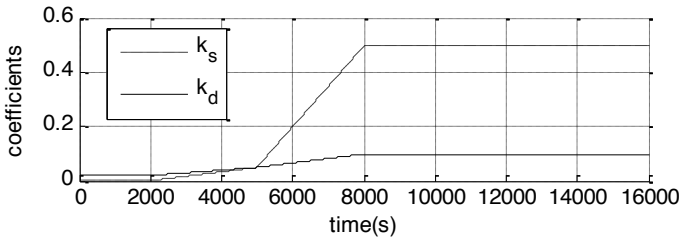

Fig. 2 Tuning of the coefficients with respect to time.

The VSDM control with Gabriel graph-based topology switching and collision avoidance was simulated. The simulation time was 16,000 s. The spacecraft's relative position with respect to the 1st spacecraft in the ECI reference frame and the connecting topology are shown in Fig. 3. The history of the relative position errors is presented in Fig. 4. The control accelerations are presented in Fig. 5. These figures show a high accuracy for maintaining formation and small control accelerations at steady state.

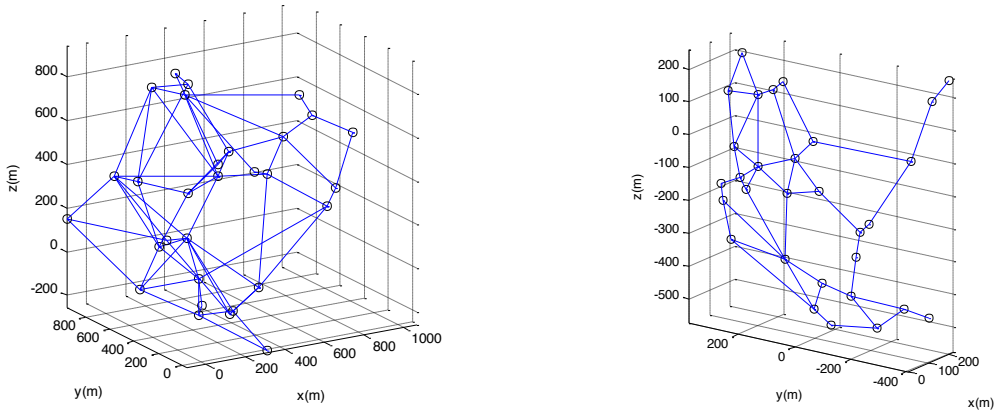

(*a*) Initial time (t = 0 s). (*b*) Steady state (t = 8000 s).

Fig. 3 Relative configuration and connecting topology of the 30 spacecraft.

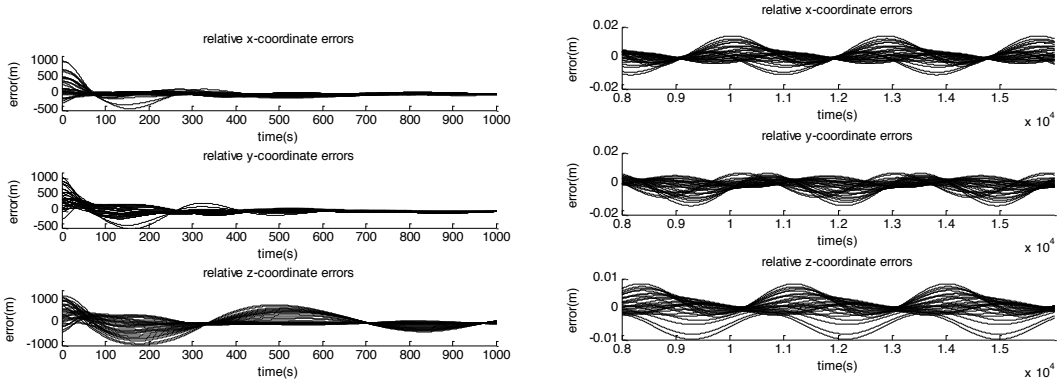

(*a*) Transient state. (*b*) Steady state.

Fig. 4 Relative position errors of the other 29 spacecraft with respect to the 1st spacecraft.

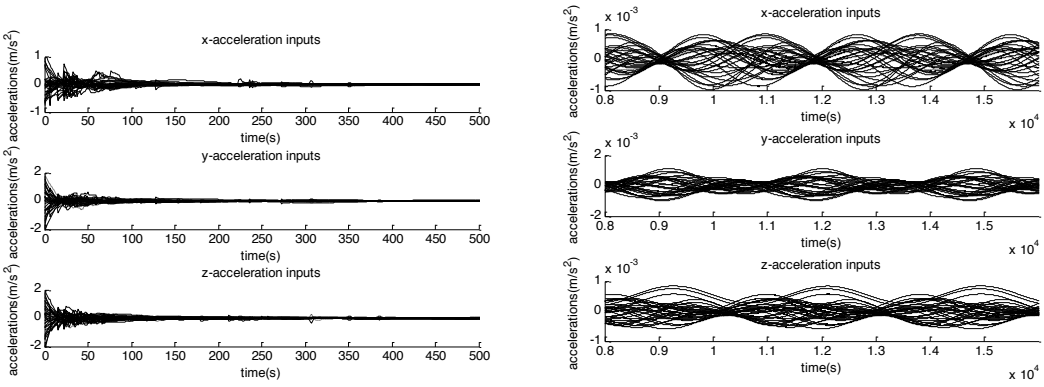

(*a*) Transient state. (*b*) Steady state.

Fig. 5 Control accelerations of the 30 spacecraft.

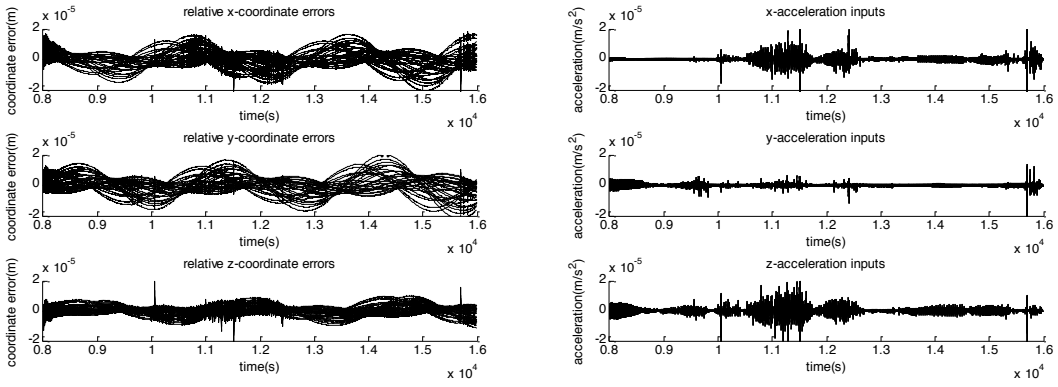

(*a*) Differences of the relative coordinate errors. (*b*) Differences of the control accelerations.

Fig. 6 Differences between the predicted steady-state performance and the simulation results.

Eqs. (20) and (22) were used to predict the steady-state errors and control accelerations, respectively. Differences between the predicted steady-state performance and the simulation results are presented in Fig. 6. It is shown that the errors of Eqs. (20) and (22) are quite small, although the equations are obtained by approximation.

The artificial potential function used to handle collision avoidance is

$$\varphi(l) = \begin{cases} k_\varphi f(\bar{l}), & 0 < \bar{l} \le 1 \\ 0, & \bar{l} > 1 \end{cases}$$

where $f(\bar{l}) = \bar{l}^{-2} - 3\bar{l}^{2} + 8\bar{l} - 6$, $\bar{l} = \left(l - l_0\right)/d$ is the normalized distance, the scaling factor $k_\varphi = -\alpha_k d / f'(\bar{l}_k)$, l_0 = 25 m, d = 10 m, $\alpha_k = 0.1$, and $\bar{l}_k = 0.5$. The collision history of the simulation case with and without collision avoidance is given in Fig. 7. By integrating the collision avoidance in the VSDM control, collisions are successfully eliminated.

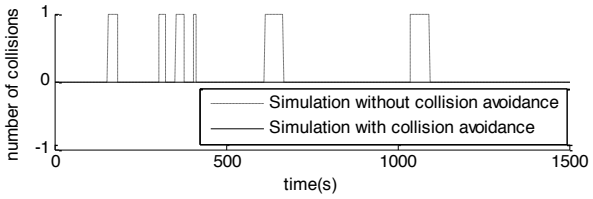

Fig. 7 Number of collisions that occurred with respect to time.

VII. Conclusion

Inspired by the physical analogy of a system of free point masses connected by spring-dampers, this paper developed a distributed formation control method for spacecraft swarms in a gravitational potential field. The convergence of the closed-loop system was proven, and approximate expressions for the relative motion errors and

control accelerations at steady-state were derived, showing that the steady-state errors can be arbitrarily small if a sufficiently large elastic coefficient is used. Collision avoidance was integrated by using artificial potential functions. A topology switching criterion that can be checked in a distributed manner was developed for the virtual spring-damper mesh-based formation control, and with the aid of Gabriel graphs, a strategy for switching to advantageous topologies was established. Numerical simulations of a 30 spacecraft formation in low Earth orbit show the effectiveness of this method. The proposed method uses only relative-state measurements and is scalable to a large number of spacecraft. The issue of virtual spring-damper mesh-based formation control using distances instead of relative states deserves further study. Following time-varying configurations, such as a rotating formation for pointing a moving target, is another topic for future work.

Acknowledgments

This work was supported by the National Natural Science Foundation of China (61273351 and 10802094).

References

[1] Mesbahi, M., and Egerstedt, M., *Graph Theoretic Methods in Multiagent Networks*, Princeton University Press, Princeton, 2010, chs. 2, 4, 6.

[2] Mesbahi, M., and Hadaegh, F. Y., "Formation Flying Control of Multiple Spacecraft via Graphs, Matrix Inequalities, and Switching," *Journal of Guidance, Control, and Dynamics*, Vol. 24, No. 2, 2001, pp. 369-377. doi: 10.2514/2.4721

[3] Tanner, H., Pappas, G., and Kumar, V., "Leader-to-formation Stability," *IEEE Transactions on Robotics and Automation*, Vol. 20, Issue 3, 2004, pp. 443–455. doi: 10.1109/ TRA.2004.825275

[4] Scharf, D. P., Hadaegh, F. Y., and Ploen, S. R., "A Survey of Spacecraft Formation Flying Guidance and Control (Part II): Control," *Proceeding of the 2004 American Control Conference*, Boston, Massachusetts, June 30 - July 2, 2004.

[5] Fax, J. A., and Murray, R. M., "Information Flow and Cooperative Control of Vehicle Formations," *IEEE Transactions on Automatic Control*, Vol. 49, No. 9, 2004, pp. 1465-1476. doi: 10.1109/TAC.2004.834433

[6] Ren, W., "Formation Keeping and Attitude Alignment for Multiple Spacecraft Through Local Interactions," *Journal of Guidance, Control and Dynamics*, Vol. 30, No. 2, 2007, pp. 633-638. doi: 10.2514/1.25629

[7] Ramirez-Riberos, J. L., Pavone, M., Frazzoli, E., and Miller, D. W., "Distributed Control of Spacecraft Formations via Cyclic Pursuit: Theory and Experiments," *Journal of Guidance, Control, and Dynamics*, Vol. 33, No. 5, 2010, pp. 1655-1669. doi: 10.2514/1.46511

[8] Arcak, M., "Passivity as a Design Tool for Group Coordination," *IEEE Transactions on Automatic Control*, Vol. 52, No. 8, 2007, pp. 1380-1390. doi: 10.1109/TAC.2007.902733

[9] Wei Ren, and Randal W. Beard, "Decentralized Scheme for Spacecraft Formation Flying via the Virtual Structure Approach," *Journal of Guidance, Control and Dynamics*, Vol. 27, No. 1, 2004, pp. 73-82. doi: 10.2514/1.9287

[10] Ren, W., and Atkins, E., "Distributed Multi-Vehicle Coordinated Control via Local Information Exchange," *International Journal of Robust and Nonlinear Control*, Vol. 17, 2007, pp. 1002-1033. doi: 10.1002/rnc.1147

[11] Smith, R. S., and Hadaegh, F. Y., "Control of Deep-Space Formation-Flying Spacecraft; Relative Sensing and Switched Information," *Journal of Guidance, Control and Dynamics*, Vol. 28, No. 1, 2005, pp. 106-114. doi: 10.2514/1.6165

[12] Shucker, B., Murphey, T., and Bennett, J. K., "An Approach to Switching Control Beyond Nearest Neighbor Rules," *Proc. of the 2006 American Control Conf*erence, Minneapolis, Minnesota, 2006, pp. 5959-5965.

[13] Zelazo, D., and Mesbahi, M., "Edge Agreement: Graph-Theoretic Performance Bounds and Passivity Analysis," *IEEE Transactions on Automatic Control*, Vol. 56, No. 3, 2011, pp. 544-555. doi: 10.1109/TAC.2010.2056730

[14] Alfriend, K. T., Vadali, S. R., Gurfil, P., How, J. P., and Breger, L. S., *Spacecraft Formation Flying: Dynamics, Control and Navigation*. Elsevier Astrodynamics Series, Elsevier, 2010, ch. 2.

[15] Coletti, M., Gabriel, S.B., "The Applicability of Dual Stage Ion Optics to Ion Engines for High Power Missions," *IEEE Transactions on Plasma Science*, Vol. 40, No. 4, 2012, pp. 1053-1063. doi: 10.1109/TPS.2012.2185953

[16] Squire, J.P., Chang-Díaz, F.R., Glover, T.W., Carter, M.D., Cassady, L.D., Chancery, W.J., etc., "VASIMR Performance Measurements at Powers Exceeding 50 kW and Lunar Robotic Mission Applications," *International Interdisciplinary Symposium on Gaseous and Liquid Plasmas,* Akiu/Sendai, Japan, September 5-6, 2008.

[17] Khalil, H. K., *Nonlinear System*, 3rd ed., Prentice Hall, New Jersey, 2002, ch. 4.

[18] Lin, H., and Antsaklis, P. J., "Stability and Stabilizability of Switched Linear Systems: A Survey of Recent Results," *IEEE Transactions on Automatic Control*, Vol. 54, No. 2, 2009, pp. 308-322. doi: 10.1109/TAC.2008.2012009

[19] Matula, D. W., and Sokal, R. R., "Properties of Gabriel Graphs Relevant to Geographic Variation Research and the Clustering of Points in the Plane," *Geographical Analysis*, Vol. 12, Issue 3, 1980, pp. 205–222. doi: 10.1111/j.1538-4632.1980.tb00031.x

[20] Golomb, S. W., and Taylor, H., "Two-Dimensional Synchronization Patterns for Minimum Ambiguity," *IEEE Transactions on Information Theory*, Vol. 28, No. 4, 1982, pp. 600-604. doi: 10.1109/TIT.1982.1056526